Rapid Quantitation of Various Therapeutic Monoclonal Antibodies Using Membranes With Fc-specific Ligands

Junyan Yang[1], Raluca Ostafe[2], Christopher J. Welch[3], Brandy Verhalen[4], Ivan L. Budyak[5], and Merlin L. Bruening[1,6*]

[1]Department of Chemical and Biomolecular Engineering, University of Notre Dame, Notre Dame, IN 46556, United States

[2]Molecular Evolution, Protein Engineering and Production Facility; Purdue Institute for Inflammation, Immunology and Infection Diseases, Purdue University, West Lafayette, IN 47907, United States

[3]Indiana Consortium for Analytical Science & Engineering (ICASE), 410 W. 10th St., # 1020H, Indianapolis, IN 46202, United States

[4]Corteva Agriscience, 8325 NW 62nd Ave, Johnston, IA 50131, United States

[5]Biopharmaceutical Research and Development, Lilly Research Laboratories, Eli Lilly and Company, Indianapolis, IN 46285, United States

[6]Department of Chemistry and Biochemistry, University of Notre Dame, Notre Dame, IN 46556, United States

*Corresponding author. mbruenin@nd.edu phone: +1 574-631-3024

ABSTRACT: Therapeutic monoclonal antibodies (mAbs) provide effective treatments for many diseases including cancer, autoimmune disorders, and, lately, COVID-19. Monitoring the concentrations of mAbs is important during their production and subsequent processing. This work demonstrates a 5-minute quantitation of most human immunoglobulin G (IgG) antibodies through capture of mAbs in membranes modified with ligands that bind to the fragment crystallizable (Fc) region. This enables binding and quantitation of most IgG mAbs. Layer-by-layer (LBL) adsorption of carboxylic acid-rich polyelectrolytes in glass-fiber membranes in 96-well plates allows functionalization of the membranes with Protein A or a peptide, oxidized Fc20 (oFc20), with high affinity for the Fc region of human IgG. mAb capture occurs in <1 minute during flow of solution through modified membranes, and subsequent binding of a fluorophore-labelled secondary antibody enables quantitation of the captured mAbs using fluorescence. The intra- and inter-plate coefficients of variations (CV) are <10% and 15%, respectively, satisfying the acceptance criteria for many assays. The limit of detection (LOD) of 15 ng/mL is on the high end of commercial enzyme-linked immunosorbent assays (ELISAs) but certainly low enough for monitoring of manufacturing solutions. Importantly, the membrane-based method requires <5 minutes, whereas ELISAs typically take at least 90 minutes. Membranes functionalized with oFc20 show greater mAb binding and lower LODs than membranes with Protein A. Thus, the membrane-based 96-well-plate assay, which is effective in diluted fermentation broths and in mixtures with cell lysates, is suitable for near real-time monitoring of the general class of human IgG mAbs during their production.

INTRODUCTION

This paper describes a method for analysis of most human or humanized IgG monoclonal antibodies (mAbs) in <5 min. The process exploits rapid mAb capture in membranes containing ligands that bind to the mAb Fc region, which makes the technique applicable to most human IgG subclasses. Binding of a fluorescently labelled secondary antibody to the captured mAb yields a concentration-dependent fluorescence signal. This approach enables rapid analysis of mAb concentrations during fermentation and processing.

Monoclonal antibodies are remarkably successful therapeutics that both alleviate symptoms and prolong patients' survival time. The global mAbs market was estimated at nearly $200 billion in 2022,[1] and it will continue to grow with the approval of more mAbs.[2, 3] Bioanalysis of mAbs is an important part of quality control during their manufacture.[4] The most common strategy for mAb quantitation employs enzyme-linked immunosorbent assays (ELISAs),[5-8] which are highly sensitive, providing a lower limit of quantitation (LLOQ) at the ng/mL[9] or even pg/mL level.[10] Researchers also used ELISAs extensively to detect and profile human antibodies targeting the SARS-CoV-2 spike proteins,[11, 12] thus providing insights on designing antibodies for COVID-19 treatments. However, ELISAs usually take more than an hour, sometimes overnight, with the majority of the time spent in long incubation steps.[8, 13]

In addition to ELISAs, industrial scientists employ liquid chromatography coupled with tandem mass spectrometry (LC-MS/MS) to quantify mAbs.[8, 14] Many studies reported capture of mAbs or antibody-drug conjugates (ADCs) on functionalized magnetic beads, digestion of the captured antibodies, and quantitation of surrogate tryptic peptides using multiple reaction monitoring (MRM).[7, 15-17] Mu et al. used this strategy to

quantify a mAb combination that targets SARS-CoV-2-spike protein.[18] The technique effectively analyzed the mAb combination extracted from the nasal-lining fluids and sera of patients. Although this method is effective and possesses a sub-microgram per mL LLOQ, the assay takes hours for sample preparation prior to injection into the LC-MS/MS system.[19] Additionally, the assay requires synthesis of stable isotope-labelled internal standards, and recovery and ion suppression need to be well characterized during method validation.[20] Monitoring of mAb production should occur in near real-time to enable management of process parameters,[21] so both ELISAs and LC-MS/MS are not ideal for this purpose.

Other simpler and quicker approaches have been employed, each with limitations. Swartz and Chen introduced a method for mAb quantitation using elastin-like-polypeptides on nanoparticles. Nanoparticle aggregation upon mAb binding creates turbidity, so the light scattering signal at 600 nm depends on the antibody concentration. The method takes a few minutes but has a LLOQ of 100 µg/mL.[22, 23] Cheng et al. reported a paper-based ELISA for protein quantitation.[24] Although the time cost is significantly shorter than in traditional ELISA, the method still required ~1 h to obtain results. They employed photolithography to create a 96-well format. A simple and rapid quantitative analysis using affinity membranes may better monitor mAb manufacturing.

Membranes serve as an important tool in biotechnology processes such as protein purification[25, 26] and polishing.[27, 28] Our group developed several methods to quantify protein concentrations using membranes containing highly specific peptide ligands.[29, 30] Flow-induced mass transport in membrane pores rapidly brings proteins to ligands immobilized on the pore surface, and vertical flow through the porous membrane should allow thorough washing. Thus, affinity membranes can capture biomolecules in residence times as short as milliseconds. Incorporation of the membranes into microfluidic devices and spin columns further facilitates the detection and capture of biomolecules.[31, 32]

The prior membrane-based devices focused on binding one specific mAb or other protein, so they enabled analyses in complex matrices such as serum.[33] Development of a membrane with affinity for any human IgG has the potential to yield a device that allows analysis of a wide range of new and existing mAbs. In practice, fermentation broths typically contain only one target mAb, so the affinity ligand does not need to distinguish among mAbs. This work aims to create a broad mAb-quantitation method by modifying membranes with Protein A or a cross-linked affinity peptide. Both of these biomolecules have affinity for the Fc region of IgG and thus bind to most IgG subclasses.[34-37] Protein A was originally discovered in bacteria that use this protein for binding IgG.[38, 39] Resins containing Protein A are an industrial staple for harvesting mAbs from cell-culture supernatant with high yield and purity.[40-42] With a newly designed Protein A resin (20–25 µm beads) with lower cross-linking, Fedorenko et al. showed improved mAb purification productivity and a decrease in buffer use.[43] Gong et al. discovered a short peptide, Fc-III-4C, with very high affinity for the human IgG Fc region (dissociation constant of 2.5 nM).[44] This high affinity along with the small size of this peptide relative to Protein A could significantly enhance IgG capture in membranes. Immobilization of Protein A and Fc-III-4C in membranes in 96-well plates should enable selective capture and fast analysis of most IgG subclasses. Compared to established, routine ELISAs, the technical advance in this work is the development of a general assay for quantitative analysis of IgG mAbs in under five min. This could provide insights into optimization of mAb production and purification in near real time.

EXPERIMENTAL SECTION

Materials. Glass-fiber membranes (A/C Glass Fiber 1 µm pore, 25 mm diameter, 254 µm thickness) and AcroPrep Advance 96 well plates (350 µL well volume, each well contains 660 µm thick glass-fiber membranes with a membrane volume of 0.033 cm^3 and nominal 1 µm pores) were acquired from Pall Corporation. Poly(acrylic acid) (PAA, average M_W ~250 kDa, 35% aqueous solution), Polyethylenimine (PEI, branched, M_W = 25 kDa), N-hydroxysuccinimide (NHS), Tween 20, Ziptips with 0.6 µL C18 resin, α-cyano-4-hydroxycinnamic acid, sodium phosphate monobasic monohydrate, sodium phosphate dibasic heptahydrate, sodium chloride, sodium hydroxide, Tris-HCl and 0.22 µm vacuum filter units were purchased from Sigma-Aldrich. N-(3-dimethylaminopropyl)-N'-ethylcarbodiimide hydrochloride (EDC), LB broth (*E. coli* culture media), CHO cell culture media, biotinylated $F(ab')_2$-goat anti-human IgG (H+L), bovine serum albumin (BSA), Eppendorf deep-well 96-well plate, human total IgG ELISA kit, PureLink™ Expi endotoxin-free maxi plasmid purification kit, ExpiCHO-S cells, ExpiFectamine CHO transfection kit, and ExpiCHO expression medium were purchased from ThermoFisher Scientific. *E. coli* cell lysate (MG1655 strain, 1.15 mg/mL total protein concentration as determined by BCA assay) was a gift from the Champion lab at the University of Notre Dame. Lyophilized Protein A was purchased from Novus Biologicals. Fc20 peptide (KGSGSCDCAWHLGELVWCTC) in reduced form was synthesized by Genscript with a purity of 95.2%. Trastuzumab (Kanjinti, Amgen), Bevacizumab (Avastin, Genentech), Rituximab (Rituxan, Genentech), and Nivolumab (Opdivo, Bristol Myers Squibb) were stored and used in their formulation buffers. Pre-adsorbed goat anti-human IgG (H+L) labelled with Cy5, pre-adsorbed goat $F(ab')_2$ anti-human IgG - $F(ab')_2$ labelled with Dylight650, streptavidin-coated gold nanoparticles (SA-GNP, 20 nm diameter, 10 OD) and Anti-HER2 ELISA kit were acquired from Abcam. HiTrap Protein A HP column 5 mL was purchased from Cytiva Life Sciences. Ultrafiltration centrifugation columns with 10 kDa exclusion limit were acquired from Sartorius. The CR3022 vH and vL sequences (GenBank: DQ168569 and DQ168570, respectively) subcloned into (pFUSEss-CHIg-hG1 and pFUSEss-CLIg-hk, respectively) for transient expression were obtained from BEI repository (reagents were produced under HHSN272201400008C and obtained through BEI Resources, NIAID, NIH: Plasmid Set for Anti-SARS Coronavirus Human Monoclonal Antibody CR3022, NR-53260). Solutions were prepared using analytical grade chemicals and deionized (DI) water (Milli-Q, 18.2 MΩ cm).

Immobilization of Protein A or oxidized Fc20 peptide in a 25 mm-Diameter Glass-Fiber Membrane. Fc20 peptide (2 mg) was dissolved in 2 mL of 20 mM phosphate buffer (pH 7.4 in 150 mM NaCl, Buffer A), and the pH of the solution was adjusted to 9.0 with 1 M NaOH. The solution was incubated overnight at room temperature with the cap left ajar to allow mild oxidation[44]. The disulfide-bond composition of oxidized Fc20 (oFc20) was elucidated using matrix-assisted laser desorption/ionization-time of flight (MALDI-TOF) mass spectrometry. Protein A was dissolved in Buffer A at a concentration of 1 mg/mL with no further treatment.

A 25 mm-diameter glass-fiber membrane was first cleaned with UV/O_3 treatment (Jelight, model 18) for 10 min.

Membrane modification employed a custom membrane holder, a peristaltic pump, and a single membrane. The O-ring in the holder reduces the exposed diameter of the membrane to 2 cm (effective bed volume of 0.080 cm^3). Five mL of DI water was passed through membrane at 1 mL/min (the flow rate is the same for all subsequent steps). Ten mL of 2 mg/mL branched PEI (pH 3.0, no salt) was then circulated through the membrane for 20 min, followed by passage of 10 mL of DI water. Ten mL of 1.1 mg/mL PAA (pH 3.0, 0.5 M NaCl) was then circulated through the membrane for 20 min before passage of 10 mL of DI water. The PEI/PAA deposition process was repeated a second time to generate $(PEI/PAA)_2$ bilayers. Five mL of 0.1 M EDC/NHS solution (equimolar) in water was next circulated through the membrane for 1 hour. After circulation, the membrane was rinsed with 10 mL of DI water, followed by circulation of 1 mL of 1 mg/mL Protein A or oFc20 solution for 1 hour. Finally, 10 mL of Buffer A was passed through membrane to remove unbound Protein A or oFc20.

The concentrations of Protein A or oFc20 in the load, permeate and washing solutions were determined from the intrinsic fluorescence of the ligand (tyrosine for Protein A and tryptophan for oFc20)[45] using a Synergy H1 microplate reader. Permeate solutions were diluted 10-fold (v:v) using Buffer A to minimize any absorbance from NHS-esters dissociated from activated membranes.[46, 47] A series of analyte standards were made by diluting stock solution using Buffer A. Tyrosine was excited at 276 nm, and fluorescence was monitored at 304 nm, whereas tryptophan was excited at 280 nm, with emission monitored at 348 nm.

Immobilization of Protein A and oFc20 in Porous Glass-fiber Membranes in 96-well Plates. The procedure for immobilization of affinity ligands in glass-fiber membranes in 96-well plates includes three parts, deposition of polyelectrolyte layers, chemical activation of functional groups, and the covalent linking of affinity ligands to glass-fiber membranes. 100 µL of 2 mg/mL branched PEI was added into each well for a 5-min incubation. Then the solutions were pulled vertically through the glass-fiber membranes using a vacuum manifold (see Figure S1 for the configuration) at a flow rate of ~5 mL/min. The PEI incubation was repeated another three times, followed by pulling 1 mL of DI water through the well. 100 µL of 1.1 mg/mL PAA in 0.5 M NaCl were added into each well for a 5-min incubation before solution was pulled through the well by vacuum at a flow rate of ~5 mL/min. After another three rounds of PAA incubation, 1 mL of DI water was pulled through the membrane. PEI and PAA deposition steps were repeated an additional time to create two PEI/PAA bilayers.

Carboxylic acid groups in adsorbed PAA were activated by adding 100 µL of solution containing 0.1 M EDC and 0.1 M NHS into each well for a 10-min incubation. After pulling the solution through the membranes using vacuum at a flow rate of ~5 mL/min, the incubation was repeated for another five times, followed by passage of 1 mL of DI water through the membrane.

Finally, to allow covalent linking between activated -COOH groups and ligands, 100 µL of 100 µg/mL Protein A solution were added into each well for a 10-min incubation. The solution was pulled through the membrane at ~5 mL/min, followed by another five Protein A incubations. The wells were finally rinsed by passing 2 mL of Buffer A followed by 1 mL of 20 mM phosphate containing 500 mM NaCl (pH 7.4, Buffer B) through the well. oFc20 was immobilized in membranes in 96-well plates following the same procedures, except 50 µg/mL oFc20 was used instead of 100 µg/mL Protein A.

Measurement of Trastuzumab Breakthrough Curves in Ligand-Modified Glass-Fiber Membranes. Using the custom holder,[30] a single 25 mm-diameter (20 mm exposed diameter in the holder) Protein A-modified glass-fiber membrane was first rinsed with 5 mL of Buffer B at 1 mL/min. Subsequently, 8 mL of 50 µg/mL Trastuzumab in Buffer B was passed through the membrane at 0.5 or 2.5 mL/min. Permeate aliquots were collected in pre-weighed tubes, and the volume of the permeate aliquot was determined based on the increase in mass. The concentration of Trastuzumab in each aliquot was determined by measuring the intrinsic tryptophan fluorescence using a Synergy H1 microplate reader. For oFc20-modified glass-fiber membranes, 12 mL of 50 µg/mL Trastuzumab solution was passed through the membrane. Otherwise, the procedure was the same.

Quantitation of Trastuzumab in Buffer Using Ligand-Modified Membranes in 96-well Plates. A series of Trastuzumab standards (0, 0.5, 1, 2, 4, 6, 8, 10 µg/mL) were prepared by diluting stock Trastuzumab solution with Buffer B. Flow rates through the plate were adjusted using test solutions in other wells by opening or closing the vacuum valve. Figure 1 schematically shows the experimental workflow for 96-well plate. Initially, 1 mL of Buffer B was passed through the well at the maximum vacuum (~5 mL/min) to equilibrate the membranes. Next, 0.5 mL of Trastuzumab standards were passed through the well at ~0.5 mL/min. After solutions were pulled through membranes, 2 mL of Buffer B was passed through the membrane at the highest vacuum to remove nonspecifically bound material. At a flow rate of 1 mL/min, 0.5 mL of 10 µg/mL goat anti-human IgG secondary antibody was passed through each well, followed by 2 mL of washing at ~5 mL/min with 20 mM phosphate containing 500 mM NaCl and 0.1% (v:v) Tween 20 (pH 7.4, Buffer C). The secondary antibody used for Protein A-modified membranes was Cy5-labelled pre-adsorbed goat anti-human IgG (H+L), and for oFc20 modified membranes the antibody was Dylight650-labelled pre-adsorbed goat $F(ab')_2$ anti-human IgG-$F(ab')_2$. The 96-well plate was inserted in the plate reader for on-membrane fluorescence measurement (Cy5: excitation 645 nm, emission at 670 nm; Dylight650: excitation 650 nm, emission 675 nm). The calibration curve was established based on the fluorescence intensity of fluorophores linked to secondary antibodies as a function of the concentration of Trastuzumab in the loading solution. A set of independent Trastuzumab samples (theoretical concentration of 1.5, 3, 5 and 7 µg/mL Trastuzumab) were also prepared, and passed through ligand-modified membranes, followed by Buffer B rinsing, secondary antibody loading and Buffer C washing, as described above. The fluorescence emission intensity was measured, and the experimental concentration was

determined using the calibration curve.

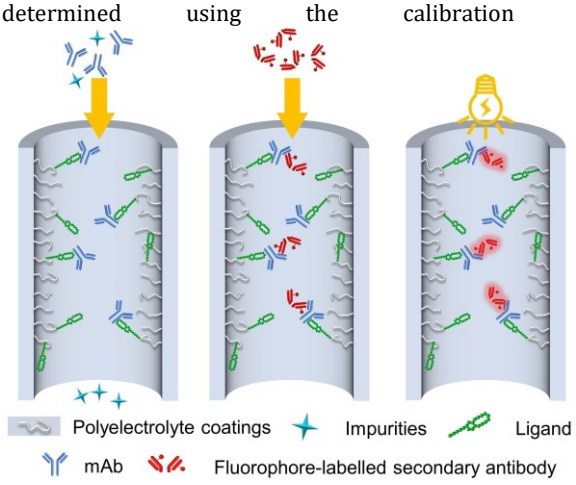

Figure 1. Scheme of the experimental workflow for mAb analysis with 96-well plates containing functionalized membranes. The procedure includes selective capture of mAbs, binding of fluorescently labelled secondary antibodies, and determination of the mAb concentration by fluorescence detection.

Quantitation of Trastuzumab from Diluted Cell Culture Media, Supernatant or Cell Lysate. Chinese hamster ovary (CHO) cell lines are widely used for mAb production due to high yields and the possibility for post-translational modifications (PTMs).[48, 49] To obtain relevant cell culture media concentrations at 10 μg/mL mAb levels, CHO cell culture media was spiked into the Trastuzumab standards and independent Trastuzumab samples at a volume ratio of 1:1000. We also deliberately added *E. coli* cell lysate to simulate contamination that would occur for proteins expressed in *E. coli*. In our experiments, we employed 150 μg/mL of *E. coli* cell lysate protein in solutions containing 0.5-10 μg/mL Trastuzumab (lysate protein was also added to the blank). Thus, the Trastuzumab constitutes 0.3 to 7 wt% of the total protein.

Binding of Gold Nanoparticles to Secondary Antibodies. Protein A- or oFc20-modified membranes in 96-well plates were loaded with 0.5 mL of 10 μg/mL Trastuzumab in Buffer B prior to rinsing and passage of 0.5 mL of 10 μg/mL biotinylated goat $F(ab')_2$ anti-human IgG (H+L). The wells were rinsed with 2 mL of Buffer C. Finally, 0.5 mL of 1:50 (v:v) diluted SA-GNPs (20 nm diameter) was passed through each well prior to rinsing with 2 mL of Buffer C and 2 mL of DI water. Membranes were removed from wells before sputter coating with ~5 nm gold/palladium and imaging using a ThermoFisher Helios G4 Ux instrument.

RESULTS AND DISCUSSION

The analytical procedure includes immobilization of ligands (Protein A or oFc20) in glass-fiber membranes, capture of a mAb, binding of a fluorophore-labelled secondary antibody, and measurement of the fluorescence from the membrane (Figure 1). The ligands bind to the Fc region of IgG to enable analysis of a wide range of human-IgG mAbs. In this section, we first describe quantitation of ligand immobilization on polyelectrolyte-modified glass-fiber membranes and examine their Trastuzumab binding capacity. Second, we investigate the capture and detection of Trastuzumab using ligand-modified membranes in 96-well plates. This process takes <5 min. Lastly, we quantify other IgG antibodies, including an anti-SARS-CoV antibody expressed in CHO cells.

Immobilization of Ligands in Glass-Fiber Membranes. To effectively bind IgGs, the Fc20 peptide must consist of monomers that contain two disulfide bonds. Thus, initially, we used MALDI-TOF MS to verify the peptide structure. As Figure S2 shows, after mild oxidation of Fc20 at room temperature, the mass spectrum of the peptide exhibits one peak corresponding to a singly charged species with a monoisotopic mass of 2150.851 Da. This mass is consistent with the loss of four hydrogens from a monomeric peptide during the formation of two intra-chain disulfide bonds. A peak for the doubly charged peptide also appeared, with no other observable peaks. Thus, after overnight oxidation, the Fc20 peptide was oxidized into a double cyclic monomer (oFc20) with two disulfide bonds. A prior study shows that the disulfide bonds are not scrambled.[44]

After elucidating the structure of oFc20, we studied the immobilization of Protein A or oFc20 in glass-fiber membranes. Protein A has long served as the standard for antibody purification,[40, 50] but oFc20, which consists of only 20 amino acids, has a higher affinity for human IgG than Protein A. The dissociation constant for the oFc20-human IgG complex is 10-fold lower than that for the Protein A-human IgG complex.[34, 44] To immobilize the ligands, we first create a high density of -COOH groups in the membrane through adsorption of $(PEI/PAA)_2$ films. EDC/NHS chemistry then allows reaction of amine groups with active esters to immobilize Protein A or oFc20 to the $(PEI/PAA)_2$ film. Crosslinking of PEI to PAA also likely occurs via EDC/NHS coupling to stabilize the coating.

To quantitatively study Protein A and oFc20 peptide immobilization, we coated a 25-mm diameter (the O-ring reduces its exposed diameter to 2 cm) glass-fiber membrane with $(PEI/PAA)_2$ bilayers using a customized membrane holder and a peristaltic pump that circulated solutions through the membrane.[29, 30] Then, a 1 mg/mL affinity-ligand solution was circulated through the membrane for 1 hour at 1 mL/min. The load, permeate and wash solutions were collected to determine the affinity-ligand concentration based on intrinsic fluorescence and to calculate the amount of immobilized affinity ligand. The results suggest immobilization of 14±1 mg of Protein A and 8±1 mg of oFc20 per mL of membrane. Uncertainties are the standard deviations from three replicate membranes for each ligand. Functionalization of 96-well plates requires a modified procedure because we could not circulate solutions through the wells. Instead, we derivatized $(PEI/PAA)_2$-modified membranes in 96-well plates using repeated incubation in solutions containing 100 μg/mL Protein A or 50 μg/mL oFc20. This might lead to decreased ligand immobilization in the membrane within the 96-well plates compared to the flowthrough method.[33] As described in Section S3, we determined immobilization of 1.0±0.1 mg of Protein A and 0.7±0.06 mg of oFc20 per mL of membrane in wells in 96-well plates. Lower ligand immobilization in the plate may stem from the lower ligand concentrations used in the modification solutions for the plates due to the ligand cost. However, the membrane in the plate is 2.6-fold thicker than the 25-mm membrane, which may aid in capturing antibodies.

Characterization of Trastuzumab Capture in Glass-Fiber Membranes Modified with Affinity Ligands. After immobilization of Protein A in 2-cm diameter glass-fiber membranes, we examined Trastuzumab binding during flow of solutions through the membrane. Figure 2A shows the breakthrough curve during passage of 8 mL of 50 μg/mL Trastuzumab through Protein A-modified membranes at different flow rates. The largely overlapping Trastuzumab breakthrough curves at

flow rates of 0.5 mL/min and 2.5 mL/min suggest that Trastuzumab binding to Protein A is fast compared to the residence times in the membranes.[51, 52] Summing the products of aliquot volume and the difference between feed and permeate concentrations gives a Trastuzumab equilibrium binding capacity of 0.9±0.2 mg per mL of membrane, where the uncertainty is the standard deviation of experiments with three different membranes using a flow rate of 0.5 mL/min. Figure S3A shows replicate breakthrough curves for Trastuzumab binding to Protein A membranes at different flow rates. Breakthrough curves during passage of BSA solution through the same membranes (Figure S3C) show minimal BSA binding, demonstrating that Protein A is highly specific for Trastuzumab.

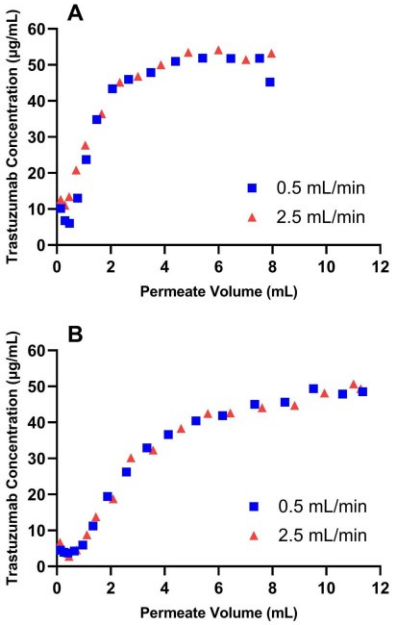

Figure 2. Breakthrough curves obtained during passage of 50 µg/mL Trastuzumab through 25 mm-diameter glass-fiber membranes modified with ligands. (A) 8 mL of Trastuzumab solution passed through Protein A-modified membranes. (B) 12 mL of Trastuzumab passed through oFc20 modified membranes at different flow rates. Blue squares and red triangles indicate 0.5 mL/min and 2.5 mL/min flow rates, respectively. The exposed membrane diameter in the holder was 2 cm.

Similarly, we explored Trastuzumab binding during passage of 50 µg/mL Trastuzumab solutions through oFc20-modified membranes at 0.5 and 2.5 mL/min. As Figure 2B shows, Trastuzumab breakthrough curves are similar at the different flow rates, suggesting rapid Trastuzumab capture in affinity membranes. Figure S3B in the supporting information shows replicate Trastuzumab breakthrough curves for oFc20-modified membranes. Comparing to Protein A-modified membranes, oFc20-modified membranes require greater volumes to achieve saturation. oFc20 membranes show an equilibrium binding capacity of 2.2±0.1 mg of Trastuzumab per mL of membrane. Figure S3D shows BSA breakthrough curves for oFc20-modified membranes, where minimal BSA binding appears.

The Protein A-modified membrane captured ~80% of the Trastuzumab in the first 0.7 mL of solution passed through it as Figure 2A shows. >80% capture corresponds to permeate concentrations <10 µg/mL. The membranes in 96-well plates have a volume that is 2.4-fold smaller than the volume of the glass-fiber membranes used to obtain breakthrough curves. Accordingly, 80% Trastuzumab capture might occur in the first 0.3 mL of solution passed through a membrane in a well. Typically, we pass 0.5 mL through the wells; therefore, complete capture likely does not occur. Moreover, the incubation method for modifying the wells may yield less binding capacity than flow-through modification. Membranes with oFc20 show greater capture than membranes with Protein A.

Affinity Membranes in 96-well Plates for Rapid Quantitation of Trastuzumab in Buffer. Next, we examine the quantitation of Trastuzumab in phosphate buffer and various matrices using affinity membranes in 96-well plates. The analysis procedure begins with passage of 0.5 mL of Trastuzumab solution through affinity membranes in 96-well plates. After washing with Buffer B, we pass 0.5 mL of 10 µg/mL fluorophore-labelled goat anti-human secondary antibody through the membrane and perform final rinse. The hands-on time for these procedures is ~2.5 min. Measurement of on-membrane fluorescence uses a microplate reader and takes < 1 min, and a plot of fluorescence as a function of the Trastuzumab concentration in the loading solution serves as a Trastuzumab calibration curve.

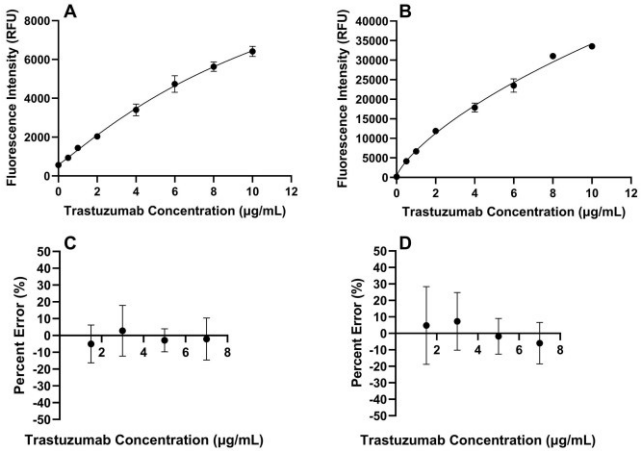

Figure 3. (A, B) Calibration curves for analysis of Trastuzumab in Buffer B using (A) Protein A-modified 96-well plates or (B) oFc20 modified 96-well plates. (C, D) Percent errors in the analyses of independent Trastuzumab solutions using (C) Protein A-based 96-well plates or (D) oFc20-based 96-well plates. The Protein-A-based assays employed a Cy5-labelled whole-form secondary antibody, whereas the oFc20-based assay used a Dylight650-labelled $F(ab')_2$ fragment secondary antibody. Error bars in the calibration curves show standard deviations from measurements with three different membranes, whereas error bars in panels C and D represent standard deviations from measurements using at least six different membranes in the same 96-well plate. Note that in some cases the symbols obscure the error bars in the calibration curves.

Figure 3A shows the Trastuzumab calibration curve (0 – 10 µg/mL in Buffer B) obtained using Protein A-modified 96-well plates. We use a four-parameter logistic fit to describe the data. As expected, the fluorescence intensity increases as the Trastuzumab concentration in the loading solution increases but not linearly. The amount of Trastuzumab binding to Protein A likely approaches saturation at the higher concentrations.[33] A control experiment with no immobilized Protein A gave little fluorescence signal (Figure S4A).

Figure 3B shows the Trastuzumab calibration curve obtained with oFc20-modified 96-well plates. These assays used a

Dylight650-labelled F(ab')$_2$ fragment secondary antibody to limit non-specific adsorption. The fluorescence intensity is ~6-fold higher than that obtained in the Protein A-based assay in Figure 3A. The higher fluorescence intensity with oFc20-modified membranes likely stems from both the high affinity of oFc20 towards the human IgG Fc region and stronger fluorescence of the Dylight650 fluorophore compared to Cy5.[53] The reported dissociation constants for oFc20- and Protein A-human IgG complexes are 2.5 and 35 nM, respectively.[34, 44] Figure S5 directly compares assays with oFc20 and Protein A membranes when using the same secondary antibody (F(ab')$_2$ fragments). The signal with the oFc20 is still 3-fold greater. A control experiment with no immobilized oFc20 gave little fluorescence signal (Figure S4B).

To make sure established calibration curves are suitable for Trastuzumab quantitation, we analyzed a set of independent Trastuzumab solutions with concentrations of 1.5, 3, 5, and 7 μg/mL Trastuzumab. Percent errors were calculated as the difference between experimental and theoretical concentrations divided by the theoretical concentration. Figure 3C shows the percent error in analyses that employ the calibration curve in Figure 3A. The average percent errors of the independent solutions are within ±10%, indicating that the Protein A-modified 96-well plate gives accurate Trastuzumab quantitation. The standard deviations of percent errors are also <15%. Such small error bars indicate the high precision of the assay. We also examined the accuracy and precision of analyses with oFc20-modified 96-well plates. As shown in Figure 3D, the percent error of independent Trastuzumab samples exhibited average percent errors with ±10%. The standard deviation in the percent error of the lowest-concentration solution is <25%, while other solutions have standard deviations <15%. The high accuracy and precision of the assay should satisfy the requirements for most analyses of Trastuzumab and other mAbs.[54-56]

The signal at 0 μg/mL Trastuzumab is relatively high in Protein-A based assays (562±41). This suggests possible non-specific binding of the goat whole-form anti-human IgG secondary antibody to Protein A, which reportedly binds weakly with the Fc region of goat antibodies.[57] To minimize non-specific binding, we began using F(ab')$_2$ fragment secondary antibodies that do not contain an Fc region,[58] so they should not bind to either oFc20 or Protein A. As Figure S6A-C shows, using the F(ab')$_2$ fragment goat secondary antibody with Protein A-modified 96-well plates decreases the blank signal compared to using the whole-form goat secondary antibody, even with the high quantum yield of the Dylight650 fluorophore. Additionally, the signal at 0 μg/mL Trastuzumab is only 178±19 for the oFc20 membranes.

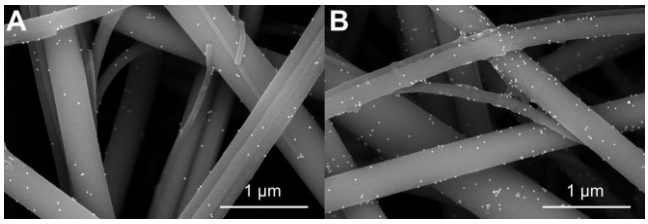

Figure 4. (A) SEM image of a Protein A-modified membrane from a 96-well plate after capture of Trastuzumab and binding of a biotinylated secondary antibody and streptavidin-GNP. (B) Image of an oFc20-modified membrane from a 96-well plate after the same treatment.

We qualitatively investigated the binding capacity of secondary antibodies with scanning electron microscopy (SEM). To do this, we bound biotinylated goat F(ab')$_2$ anti-human IgG (H+L) to Trastuzumab-loaded membranes, and subsequently passed 0.5 mL of 1:50 (v:v) diluted SA-GNPs (20 nm diameter). Figure 4 shows the SEM images of Protein A- and oFc20-modified membranes after capture of SA-GNPs. The particles appear bright due to the reflection of electrons in the back-scattering mode,[59, 60] and their diameters match the nominal value of 20 nm. In these and other replicate images (Figure S7A-H), more GNPs appear on oFc20 modified membranes than on Protein A modified membranes. The images suggest that oFc20 membranes capture more Trastuzumab than Protein A membranes, and, hence, secondary antibody binding is also higher with the high-affinity oFc20 than Protein A. This is consistent with the breakthrough curves, which show a higher binding capacity with oFc20 compared to Protein A.

Analysis of Trastuzumab in Matrices Relevant to mAb manufacturing. To examine the possibility of near real-time quantification of mAbs during fermentation, we explored the performance of affinity membranes in solutions spiked with CHO cell culture media. CHO cell lines can produce up to 10 g/L of mAbs under an optimized fermentation environment.[49, 61] To correlate with the dynamic range in this work (<10 μg/mL), we performed analysis in 1:1000 (v:v) diluted CHO-culture media in Buffer B. Figure S8A shows the calibration curve for Trastuzumab containing 1:1000 diluted CHO-culture media and analyzed using Protein A-modified 96-well plates. The calibration curve is similar to that in phosphate buffer (compare Figure 3A and Figure S8A). Analyses of independent samples spiked with diluted CHO-culture media show average percent errors within ±10%, while the standard deviation of percent errors is <15%, as suggested in Figure S8C. Thus, Protein A-modified 96-well plates exhibit high accuracy and precision for quantifying Trastuzumab in diluted CHO-culture media. oFc20-modified membranes show similar agreement between analyses in buffer and buffer spiked with CHO-culture media (see Figure S8B and S8D).

We also explored Trastuzumab analysis in solutions spiked with *E. coli* cell lysate to demonstrate selectivity. *E. coli* cells excrete limited amounts of the protein of interest to the cell culture fluids, so purification of recombinant proteins typically includes cell lysis. A total protein concentration of 150 mg/mL was reported for *E. coli* cells at 10^9 cells/L.[62] We spiked diluted *E. coli* cell lysate into Trastuzumab solutions to generate a total protein concentration of ~150 μg/mL. In this case, the protein of interest is 6.7 wt% of total protein at most, which is a reasonable estimate for protein expression in *E. coli* cell lines. Figure S9A shows the Trastuzumab calibration curve in spiked *E. coli* cell lysate when using Protein A-modified plates, and Figure S9B shows the error analyses of independent samples using this calibration curve. Figure S9C and S9D show similar results for oFc20 plates. The small average errors and low standard deviation of independent samples in both assays indicate high assay accuracy and precision. Notably, with spiked *E. coli* cell lysate, we observe the lowest standard deviation of independent samples among all of the matrices. Thus, ligand-modified 96-well plates are suitable for quantifying Trastuzumab in diluted *E. coli* cell lysate.

Quantification of various mAbs. To demonstrate that our assay can quantify various mAbs, we examined membrane-based analysis of three other therapeutic mAbs in phosphate buffer. Bevacizumab is a humanized IgG1 antibody, and its Fc region

has the same amino acid sequence as Trastuzumab.[63, 64] Despite the differences in the Fab sequences in Bevacizumab and Trastuzumab, Protein A and oFc20 should enable quantitation of both mAbs. Rituximab is a chimeric human IgG1 antibody.[65] Its Fab region contains mostly murine sequence, but the Fc region contains the human sequence. However, its Fc sequence is slightly different than those of Bevacizumab and Trastuzumab.[66] We expect assays using Protein A and oFc20 to effectively quantify Rituximab through binding to the humanized Fc region. Nivolumab is a fully human IgG4 antibody[67], so it possesses a different Fc region than IgG1. Nevertheless, Protein A retains its binding affinity towards Human IgG4. Thus, we expect our affinity membranes to effectively quantify Nivolumab.

Figure S10A-D in the supporting information shows the calibration curves of Trastuzumab, Bevacizumab, Rituximab and Nivolumab, respectively. Both Protein A and oFc20-modified membranes yield fluorescence signals that increase with mAb concentration for all of these mAbs. Surprisingly, the oFc20-modified 96-well plates can quantify Rituximab, even though it possesses a largely murine $F(ab')_2$ region. The goat anti-human $F(ab')_2$ secondary antibody used in these analyses targets the human IgG $F(ab')_2$ region. The fluorophore-labelled secondary antibody apparently has affinity for the murine $F(ab')_2$ region, likely because of sufficient similarity to the human sequence.

Comparison with ELISAs. Due to their high specificity and sensitivity, ELISAs are among the most popular techniques for mAb quantitation. Their LOD typically ranges from pg/mL to ng/mL. To compare our assays using modified membranes in 96-well plates with commercial ELISAs, we first determined the LOD of our assays. The Trastuzumab calibration curves in Figure 3A and Figure 3B, give a LOD of 60 and 15 ng/mL for assays with Protein A- oFc20-modified membranes, respectively. We calculated the detection limit as 3.3 times the standard deviation of the blank signal divided by the slope of the calibration curve at the lowest concentrations. To investigate the quantitation of Trastuzumab at ng/mL levels, we also prepared a calibration curve using eight standards with concentrations ranging from 0-1,000 ng/mL. Figure 5A shows the Trastuzumab calibration curve for Protein A-modified 96-well plates. Using this calibration curve, we determined the concentrations of four independent Trastuzumab solutions with concentrations of 1- to 9-times the LOD of 60 ng/mL. Figure 5B shows that even at concentrations just 3 times the nominal detection limit, we could effectively quantify Trastuzumab. The average percent errors and standard deviation of percent error fall within ±20% for all independent Trastuzumab samples with concentrations >180 ng/mL. This is consistent with a LLOQ that is 3×LOD = 180 ng/mL.

For oFc20-based assays, Figure 5C and 5D demonstrate effective quantitation even at 45 ng/mL Trastuzumab. Thus, the LLOQ of this assay is approximately 3×LOD, which is 45 ng/mL. Moreover, with both Protein A- and oFc20-modified membranes, linear calibration is possible. At these low concentrations, the binding does not approach saturation, so the amount of captured Trastuzumab varies linearly with concentration.

To compare with ELISAs for mAb quantitation, we performed anti-HER2 ELISAs and human total IgG ELISAs with commercial kits following the manufacturer's protocol.[68, 69] Figure S11A shows the Trastuzumab calibration curve using anti-HER2 ELISA. The LLOQ is 0.6 ng/mL, and the manufacturer reports a LLOQ value of 11 ng/mL. The latter value is comparable to the detection limit of the oFc20-based assay. As suggested by the Trastuzumab calibration using human total IgG ELISA in Figure S11C, the LLOQ is 0.6 ng/mL, and the manufacturer reports a value of 2 ng/mL. Although the LLOQ of human total IgG ELISA kits is lower than with either Protein A- or oFc20-modified 96-well plates, the hands-on time is 80 or 110 min for the ELISAs but 3 min for the membrane-based methods. The ELISA kits give approximately the same level of uncertainties in quantitation as affinity membrane-based 96 well plates (see Figure S11B and S11D in the supporting information). The intra- and inter-plate CVs of the ELISA kits were reported as <15%. We found an intra-plate CV of 4.7% for anti-HER2 ELISA and 8.6% for human total IgG ELISA. As Table S1 shows, the ligand-modified 96-well plates, especially the oFc20-based assay, are comparable to the commercial ELISA kits in many aspects, with a significant reduction in assay time.

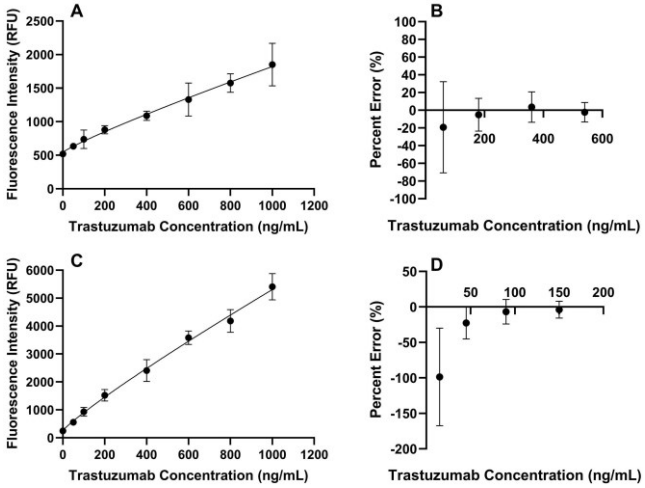

Figure 5. (A) Calibration curve for Trastuzumab (0-1000 ng/mL) analysis with Protein A-modified 96-well plates. (B) Percent errors in the analysis of independent solutions. The independent Trastuzumab solutions contain Trastuzumab concentrations equal to 1, 3, 6, and 9 times the LOD of 60 ng/mL. (C) Calibration curve for Trastuzumab (0-1,000 ng/mL) analysis with oFc20-modified 96-well plates. (D) Percent errors in the analysis of independent solutions. The independent Trastuzumab solutions contain Trastuzumab concentrations equal to 1, 3, 6, and 10 times the LOD of 15 ng/mL. All calibration curves contain data from at least three different membranes. A four-parameter logistic fit was applied for curve fitting. Independent samples contain at least six replicates.

Quantitation of A Monoclonal Antibody Harvested from Clarified CHO-Culture Supernatant. This section investigates quantitation of a human IgG1 monoclonal antibody to SARS-CoV spike protein CR3022 clone (denoted as Ab3022). The supporting information describes procedures for transfection, cell culture and supernatant collection. CHO-culture supernatant was collected on day 3 and 7 of cell culture, and supernatant from a batch of high-density CHO cells (10^7 cells/mL) cultured without transfection was also collected and denoted as the blank. We first determined the concentrations of Ab3022 in blank, day 3 and day 7 samples using a human total IgG ELISA kit. Purified Ab3022 was used to prepare standards. Figure S12 shows the ELISA calibration curve for Ab3022. We determined Ab3022 concentrations of 0, 3.7±0.2 and 56±5.5 μg/mL for blank, day 3 and day 7 samples, respectively.

To investigate the oFc20-based assay in mAb quantitation in clarified CHO supernatant, we prepared Ab3022 calibration curves using eight standards (spiked mAb in 1:9 (v:v) diluted blank CHO-culture supernatant) with Ab3022 concentrations ranging from 0-1000 ng/mL. We used this calibration curve to quantify Ab3022 in the day 3 sample after a 1:9 (v:v) dilution using Buffer B. Figure 6A shows the calibration curve using oFc20-modified 96-well plates with four replicate membranes for each concentration. A four-parameter logistic regression was applied to fit the curve and used to determine a Ab3022 concentration of 3.9±0.5 μg/mL in the undiluted day 3 supernatant. We also determined a Ab3022 concentration of 0.03±0.03 μg/mL in the blank supernatant. The black dot in Figure 6C represents the error analysis of Ab3022 quantitation in the day 3 sample. The uncertainty bar is the standard deviation of errors from six replicate membranes, and the average Ab3022 concentration obtained from ELISA served as the theoretical concentration. Within experimental uncertainty, ELISA and the 96-well method give the same concentration.

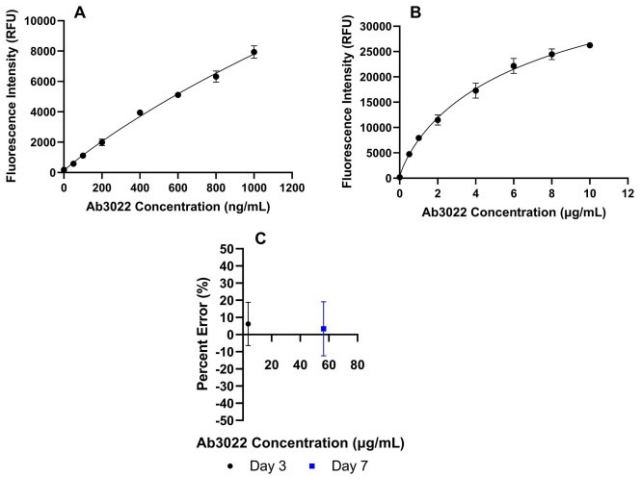

Figure 6. Calibration curves for analyzing Ab3022 in (A) 0-1000 ng/mL and (B) 0-10 μg/mL concentration ranges using oFc20-modified 96-well plates. Standards were spiked in 1:9 (v:v) diluted blank CHO-culture supernatant. (C) Error analyses of Ab3022 concentrations in 1:9 (v:v) diluted day 3 and day 7 CHO-culture supernatants. Concentrations determined from ELISA served as theoretical concentrations for each sample. Calibration curves include measurements from four different replicate wells for each concentration, and the quantitation of day 3 and day 7 samples employed six replicate wells.

Similarly, we generated an Ab3022 calibration curve with standard concentrations from 0-10 μg/mL and used it to quantify the day 7 supernatant diluted 1:9 (v:v) with Buffer B. Standards contain 1:9 diluted blank CHO-culture supernatant as background. Figure 6B shows the calibration curve, and the blue square in Figure 6C represents the error analysis of Ab3022 quantitation in the day 7 sample. The error bar is the standard deviation of errors from six replicates. We determined an Ab3022 concentration of 58±9 in the CHO-culture supernatant in the day 7 Sample. The low average percent errors and relatively small error bars in Figure 6C confirm that the oFc20-based assay can confidently quantify mAb in 10-fold diluted CHO-culture supernatant. Importantly, the oFc20-based assay takes <5 min, whereas the ELISAs require at least an hour. The oFc20-based assay could provide near real-time monitoring of mAb manufacturing.

CONCLUSION

This study demonstrates two assays suitable for mAb quantitation in under 5 min, and these assays are appropriate for several subclasses of mAbs. Protein A- or oFc20-functionalized 96-well plates can capture mAbs during the passage of solution through the plate using vacuum. Fluorophore-labelled secondary antibodies enable the detection of captured mAbs. These assays can occur in various matrices including buffer, diluted culture media and cell lysate. The detection limit for the oFc20-based assay is 15 ng/mL, with a working quantitation range from 50 ng/mL to ~8 μg/mL. Compared to well-established ELISAs, detection limits are an order of magnitude higher with the 96-well plates, but CVs are similar. Most importantly, the membrane-based assays require <5 min, whereas the ELISAs take more than an hour. Analysis of Ab3022 harvested from CHO cells demonstrates that the assay is effective under typical cell culture conditions. Future studies may focus on eluting captured mAbs for analysis of critical post-translational modifications using LC-MS/MS. To conclude, these assays may provide a general method for near real-time monitoring of most IgGs during production.

ASSOCIATED CONTENT

Supporting Information

The Supporting Information is available free of charge on the ACS Publications website.

Mass spectrum of oFc20 peptide, additional breakthrough curves, SEM images of the membranes, calibration curves and error analyses of antibodies and CVs of the assays. (PDF).

AUTHOR INFORMATION

Corresponding Author

* **Merlin L. Bruening** – Department of Chemical and Biomolecular Engineering, University of Notre Dame, Notre Dame, Indiana 46556, United States; orcid.org/0000-0002-4553-5143; Phone: +1 574-631-3024; Email: mbruenin@nd.edu

Author Contributions

The manuscript was written through contributions of all authors. / All authors have given approval to the final version of the manuscript.

ACKNOWLEDGMENT

The authors are grateful to the National Science Foundation (Grant IIP-2122540) and the NSF IUCRC Center for Bioanalytical Metrology (1916601) for funding of this work. We thank Tatyana Orlova of the Notre Dame Integrated Imaging Facility for performing SEM imaging, and Kendall A. Ryan for his help with MALDI-TOF analysis. We are grateful to Daniel Hu from the Champion lab at the University of Notre Dame for preparing *E. coli* cell lysate. We thank Ningguan Sun and Hui Yin Tan for conducting pilot studies for this project, and Qicheng Zhang for his help on graphic design.

REFERENCES

(1) Grilo, A. L.; Mantalaris, A. The Increasingly Human and Profitable Monoclonal Antibody Market. *Trends Biotechnol.* **2019**, 37, 9-16. DOI: 10.1016/j.tibtech.2018.05.014

(2) Ecker, D. M.; Jones, S. D.; Levine, H. L. The Therapeutic Monoclonal Antibody Market. *MAbs* **2015**, 7, 9-14. DOI: 10.4161/19420862.2015.989042

(3) Nelson, A. L.; Dhimolea, E.; Reichert, J. M. Development Trends for Human Monoclonal Antibody Therapeutics. *Nat. Rev. Drug Discov.* **2010**, 9, 767-774. DOI: 10.1038/nrd3229

(4) European Medicines Agency. Production and Quality Control of Monoclonal Antibodies. https://www.ema.europa.eu/en/documents/scientific-guideline/production-quality-control-monoclonal-antibodies-en.pdf (Accessed 2023-01-10).

(5) Abcam. Bevacizumab ELISA Kit (ab237642). https://www.abcam.com/bevacizumab-elisa-kit-ab237642.html (Accessed 2023-01-10).

(6) Abcam. Rituximab ELISA Kit (ab237640). https://www.abcam.com/rituximab-elisa-kit-ab237640.html (Accessed 2023-01-10).

(7) Fernandez Ocana, M.; James, I. T.; Kabir, M.; Grace, C.; Yuan, G.; Martin, S. W.; Neubert, H. Clinical Pharmacokinetic Assessment of An Anti-MAdCAM Monoclonal Antibody Therapeutic by LC-MS/MS. *Anal. Chem.* **2012**, 84, 5959-5967. DOI: 10.1021/ac300600f

(8) Ezan, E.; Bitsch, F. Critical Comparison of MS and Immunoassays for The Bioanalysis of Therapeutic Antibodies. *Bioanalysis* **2009**, 1, 1375-1388. DOI: 10.4155/bio.09.121

(9) Abcam. Pembrolizumab ELISA Kit (ab237652). https://www.abcam.com/pembrolizumab-elisa-kit-ab237652.html (Accessed 2023-01-10).

(10) Abcam. Human CD33 ELISA Kit (ab283542). https://www.abcam.com/human-cd33-elisa-kit-ab283542.html (Accessed 2023-01-10).

(11) Zost, S. J. et al. Rapid Isolation and Profiling of A Diverse Panel of Human Monoclonal Antibodies Targeting The SARS-CoV-2 Spike Protein. *Nat. Med.* **2020**, 26, 1422-1427. DOI: 10.1038/s41591-020-0998-x

(12) Zost, S. J. et al. Potently Neutralizing and Protective Human Antibodies Against SARS-CoV-2. *Nature* **2020**, 584, 443-449. DOI: 10.1038/s41586-020-2548-6

(13) Hosseni, S.; Vázquez-Villegas, P.; Rito-Palomares, M.; Martinez-Chapa, S. Enzyme-linked Immunosorbent Assay (ELISA). In *SpringerBriefs in Applied Sciences and Technology*. Springer **2018**; pp 1-18. DOI: 10.1007/978-981-10-6766-2_1.

(14) Li, H.; Ortiz, R.; Tran, L.; Hall, M.; Spahr, C.; Walker, K.; Laudemann, J.; Miller, S.; Salimi-Moosavi, H.; Lee, J. W. General LC-MS/MS Method Approach to Quantify Therapeutic Monoclonal Antibodies Using A Common Whole Antibody Internal Standard With Application to Preclinical Studies. *Anal. Chem.* **2012**, 84, 1267-1273. DOI: 10.1021/ac202792n

(15) Chiu, H. H.; Tsai, Y. J.; Lo, C.; Lin, C. H.; Tsai, I. L.; Kuo, C. H. Development of An Efficient mAb Quantification Assay by LC-MS/MS Using Rapid On-Bead Digestion. *Anal. Chim. Acta* **2022**, 1193, 339319. DOI: 10.1016/j.aca.2021.339319

(16) Hyung, S. J.; Leipold, D. D.; Lee, D. W.; Kaur, S.; Saad, O. M. Multiplexed Quantitative Analysis of Antibody-Drug Conjugates with Labile CBI-Dimer Payloads In Vivo Using Immunoaffinity LC-MS/MS. *Anal. Chem.* **2022**, 94, 1158-1168. DOI: 10.1021/acs.analchem.1c04338

(17) Dong, L.; Bebrin, N.; Piatkov, K.; Abdul-Hadi, K.; Iwasaki, S.; Qian, M. G.; Wei, D. An Automated Multicycle Immunoaffinity Enrichment Approach Developed for Sensitive Mouse IgG1 Antibody Drug Analysis in Mouse Plasma Using LC/MS/MS. *Anal. Chem.* **2021**, 93, 6348-6354. DOI: 10.1021/acs.analchem.1c00698

(18) Mu, R.; Huang, Y.; Bouquet, J.; Yuan, J.; Kubiak, R. J.; Ma, E.; Naser, S.; Mylott, W. R., Jr.; Ismaiel, O. A.; Wheeler, A. M.; Burkart, R.; Cortes, D. F.; Bruton, J.; Arends, R. H.; Liang, M.; Rosenbaum, A. I. Multiplex Hybrid Antigen-Capture LC-MRM Quantification in Sera and Nasal Lining Fluid of AZD7442, a SARS-CoV-2-Targeting Antibody Combination. *Anal. Chem.* **2022**, 94, 14835-14845. DOI: 10.1021/acs.analchem.2c01320

(19) Huang, Y.; Del Nagro, C. J.; Balic, K.; Mylott, W. R., Jr.; Ismaiel, O. A.; Ma, E.; Faria, M.; Wheeler, A. M.; Yuan, M.; Waldron, M. P.; Peay, M. G.; Cortes, D. F.; Roskos, L.; Liang, M.; Rosenbaum, A. I. Multifaceted Bioanalytical Methods for the Comprehensive Pharmacokinetic and Catabolic Assessment of MEDI3726, an Anti-Prostate-Specific Membrane Antigen Pyrrolobenzodiazepine Antibody-Drug Conjugate. *Anal. Chem.* **2020**, 92, 11135-11144. DOI: 10.1021/acs.analchem.0c01187

(20) Stokvis, E.; Rosing, H.; Beijnen, J. H. Stable Isotopically Labeled Internal Standards in Quantitative Bioanalysis Using Liquid Chromatography/Mass Spectrometry: Necessity or Not? *Rapid Commun. Mass. Spectrom.* **2005**, 19, 401-407. DOI: 10.1002/rcm.1790

(21) Rudt, M.; Brestrich, N.; Rolinger, L.; Hubbuch, J. Real-Time Monitoring and Control of The Load Phase of A Protein A Capture Step. *Biotechnol. Bioeng.* **2017**, 114, 368-373. DOI: 10.1002/bit.26078

(22) Swartz, A. R.; Chen, W. Rapid Quantification of Monoclonal Antibody Titer in Cell Culture Harvests by Antibody-Induced Z-ELP-E2 Nanoparticle Cross-Linking. *Anal. Chem.* **2018**, 90, 14447-14452. DOI: 10.1021/acs.analchem.8b04083

(23) Swartz, A. R.; Sun, Q.; Chen, W. Ligand-Induced Cross-Linking of Z-Elastin-like Polypeptide-Functionalized E2 Protein Nanoparticles for Enhanced Affinity Precipitation of Antibodies. *Biomacromolecules* **2017**, 18, 1654-1659. DOI: 10.1021/acs.biomac.7b00275

(24) Cheng, C.-M.; Martinez, A. W.; Gong, J.; Mace, C. R.; Phillips, S. T.; Carrilho, E.; Mirica, K. A.; Whitesides, G. M. Paper-Based ELISA. *Angew. Chem.* **2010**, 122, 4881-4884. DOI: 10.1002/anie.201001005

(25) Chenette, H. C.; Robinson, J. R.; Hobley, E.; Husson, S. M. Development of High-Productivity, Strong Cation-Exchange Adsorbers for Protein Capture by Graft Polymerization From Membranes With Different Pore Sizes. *J. Membr. Sci.* **2012**, 432-424, 43-52. DOI: 10.1016/j.memsci.2012.07.040

(26) Li, Y.; Lock, L. L.; Mills, J.; Ou, B. S.; Morrow, M.; Stern, D.; Wang, H.; Anderson, C. F.; Xu, X.; Ghose, S.; Li, Z. J.; Cui, H. Selective Capture and Recovery of Monoclonal Antibodies by Self-Assembling Supramolecular Polymers of High Affinity for Protein Binding. *Nano Lett.* **2020**, 20, 6957-6965. DOI: 10.1021/acs.nanolett.0c01297

(27) Osuofa, J.; Henn, D.; Zhou, J.; Forsyth, A.; Husson, S. M. High-Capacity Multimodal Anion-Exchange Membranes for Polishing of Therapeutic Proteins. *Biotechnol. Prog.* **2021**, 37, e3129. DOI: 10.1002/btpr.3129

(28) Li, Z.; Gu, Q.; Coffman, J. L.; Przybycien, T.; Zydney, A. L. Continuous Precipitation for Monoclonal Antibody Capture Using Countercurrent Washing by Microfiltration. *Biotechnol. Prog.* **2019**, 35, e2886. DOI: 10.1002/btpr.2886

(29) Berwanger, J. D.; Tan, H. Y.; Jokhadze, G.; Bruening, M. L. Determination of the Serum Concentrations of the Monoclonal Antibodies Bevacizumab, Rituximab, and Panitumumab Using Porous Membranes Containing Immobilized Peptide Mimotopes. *Anal. Chem.* **2021**, 93, 7562-7570. DOI: 10.1021/acs.analchem.0c04903

(30) Liu, W.; Bennett, A. L.; Ning, W.; Tan, H. Y.; Berwanger, J. D.; Zeng, X.; Bruening, M. L. Monoclonal Antibody Capture and Analysis Using Porous Membranes Containing Immobilized Peptide Mimotopes. *Anal. Chem.* **2018**, 90, 12161-12167. DOI: 10.1021/acs.analchem.8b03183

(31) Berwanger, J. D.; Lake, M. A.; Ganguly, S.; Yang, J.; Welch, C. J.; Linnes, J. C.; Bruening, M. Microporous Affinity Membranes and Their Incorporation Into Microfluidic Devices for Monitoring of

Therapeutic Antibodies. *Talanta* **2023**, 252, 123842. DOI: 10.1016/j.talanta.2022.123842

(32) Liu, W.; Pang, Y.; Tan, H. Y.; Patel, N.; Jokhadze, G.; Guthals, A.; Bruening, M. L. Enzyme-Containing Spin Membranes for Rapid Digestion and Characterization of Single Proteins. *Analyst* **2018**, 143, 3907-3917. DOI: 10.1039/C8AN00969D

(33) Tan, H. Y.; Yang, J.; Linnes, J. C.; Welch, C. J.; Bruening, M. L. Quantitation of Trastuzumab and an Antibody to SARS-CoV-2 in Minutes Using Affinity Membranes in 96-Well Plates. *Anal. Chem.* **2022**, 94, 884-891. DOI: 10.1021/acs.analchem.1c03654

(34) Saha, K.; Bender, F.; Gizeli, E. Comparative Study of IgG Binding to Proteins G and A: Nonequilibrium Kinetic and Binding Constant Determination With the Acoustic Waveguide Device. *Anal. Chem.* **2003**, 75, 835-842. DOI: 10.1021/ac0204911

(35) Zhao, W.-W.; Liu, F.-F.; Shi, Q.-H.; Dong, X.-Y.; Sun, Y. Biomimetic Design of Affinity Peptide Ligands for Human IgG Based on Protein A-IgG Complex. Biochem. Eng. J. **2014**, 88, 1-11. DOI: 10.1016/j.bej.2014.03.015

(36) Zhao, W. W.; Liu, F. F.; Shi, Q. H.; Sun, Y. Octapeptide-Based Affinity Chromatography of Human Immunoglobulin G: Comparisons of Three Different Ligands. *J. Chromatogr. A* **2014**, 1359, 100-111. DOI: 10.1016/j.chroma.2014.07.023

(37) Naik, A. D.; Menegatti, S.; Gurgel, P. V.; Carbonell, R. G. Performance of Hexamer Peptide Ligands for Affinity Purification of Immunoglobulin G From Commercial Cell Culture Media. *J. Chromatogr. A* **2011**, 1218, 1691-1700. DOI: 10.1016/j.chroma.2010.11.071

(38) Cruz, A. R.; Boer, M. A. D.; Strasser, J.; Zwarthoff, S. A.; Beurskens, F. J.; de Haas, C. J. C.; Aerts, P. C.; Wang, G.; de Jong, R. N.; Bagnoli, F.;Van Strijp, J. A. G.; Van Kessel, K. P. M.; Schuurman, J.; Preiner, J.; Heck, A. J. R.; Rooijakkers, S. H. M. Staphylococcal Protein A Inhibits Complement Activation by Interfering With IgG Hexamer Formation. *Proc. Natl. Acad. Sci. U S A* **2021**, 118, e2016772118. DOI: 10.1073/pnas.2016772118

(39) Keener, A. B.; Thurlow, L. T.; Kang, S.; Spidale, N. A.; Clarke, S. H.; Cunnion, K. M.; Tisch, R.; Richardson, A. R.; Vilen, B. J. Staphylococcus aureus Protein A Disrupts Immunity Mediated by Long-Lived Plasma Cells. *J. Immunol.* **2017**, 198, 1263-1273. DOI: 10.4049/jimmunol.1600093

(40) Hober, S.; Nord, K.; Linhult, M. Protein A Chromatography for Antibody Purification. *J. Chromatogr. B Analyt. Technol. Biomed. Life Sci.* **2007**, 848, 40-47. DOI: 10.1016/j.jchromb.2006.09.030

(41) Roque, A. C.; Silva, C. S.; Taipa, M. A. Affinity-Based Methodologies and Ligands for Antibody Purification: Advances and Perspectives. *J. Chromatogr. A* **2007**, 1160, 44-55. DOI: 10.1016/j.chroma.2007.05.109

(42) Gagnon, P. Technology Trends in Antibody Purification. *J. Chromatogr. A* **2012**, 1221, 57-70. DOI: 10.1016/j.chroma.2011.10.034

(43) Fedorenko, D.; Dutta, A. K.; Tan, J.; Walko, J.; Brower, M.; Pinto, N. D. S.; Zydney, A. L.; Shinkazh, O. Improved Protein A Resin for Antibody Capture in A Continuous Countercurrent Tangential Chromatography System. *Biotechnol. Bioeng.* **2020**, 117, 646-653. DOI: 10.1002/bit.27232

(44) Gong, Y.; Zhang, L.; Li, J.; Feng, S.; Deng, H. Development of the Double Cyclic Peptide Ligand for Antibody Purification and Protein Detection. *Bioconjug. Chem.* **2016**, 27, 1569-1573. DOI: 10.1021/acs.bioconjchem.6b00170

(45) Zhu, Z.; Lies, M.; Silzel, J. Native Fluorescence Detection With A Laser Driven Light Source for Protein Analysis in Capillary Electrophoresis. *Anal. Chim. Acta* **2021**, 1183, 338936. DOI: 10.1016/j.aca.2021.338936

(46) ThermoFisher. Instructions: NHS and Sulfo-NHS. https://tools.thermofisher.com/content/sfs/manuals/MAN0011309_NHS_SulfoNHS_UG.pdf (Accessed 2023-01-10).

(47) Klykov, O.; Weller, M. G. Quantification of N-hydroxysuccinimide and N-hydroxysulfosuccinimide by Hydrophilic Interaction Chromatography (HILIC). *Analytical Methods* **2015**, 7, 6443-6448. DOI: 10.1039/C5AY00042D

(48) Andersen, D. C.; Krummen, L. Recombinant Protein Expression for Therapeutic Applications. *Curr. Opin. Biotechnol.* **2002**, 13, 117-123. DOI: 10.1016/s0958-1669(02)00300-2

(49) Tihanyi, B.; Nyitray, L. Recent Advances in CHO Cell Line Development for Recombinant Protein Production. *Drug Discov. Today Technol.* **2020**, 38, 25-34. DOI: 10.1016/j.ddtec.2021.02.003

(50) Amritkar, V.; Adat, S.; Tejwani, V.; Rathore, A.; Bhambure, R. Engineering Staphylococcal Protein A for High-Throughput Affinity Purification of Monoclonal Antibodies. *Biotechnol. Adv.* **2020**, 44, 107632. DOI: 10.1016/j.biotechadv.2020.107632

(51) Anuraj, N.; Bhattacharjee, S.; Geiger, J. H.; Baker, G. L.; Bruening, M. L. An All-Aqueous Route to Polymer Brush-Modified Membranes With Remarkable Permeabilites and Protein Capture Rates. *J. Membr. Sci.* **2012**, 389, 117-125. DOI: 10.1016/j.memsci.2011.10.022

(52) Bhattacharjee, S.; Dong, J.; Ma, Y.; Hovde, S.; Geiger, J. H.; Baker, G. L.; Bruening, M. L. Formation of High-Capacity Protein-Adsorbing Membranes Through Simple Adsorption of Poly(acrylic acid)-Containing Films at Low pH. *Langmuir* **2012**, 28, 6885-6892. DOI: 10.1021/la300481e

(53) ThermoFisher. DyLight™ 650 NHS Ester. https://www.thermofisher.com/order/catalog/product/62265 (Accessed 2023-01-10).

(54) U.S. Department of Health and Human Services, F. D. A. Bioanalytical Method Validation: Guidance for Industry. **2018**. https://www.fda.gov/media/70858/download (Accessed 2023-01-10).

(55) Guidance for the Validation of Analytical Methodology and Calibration of Equipment used for Testing of Illicit Drugs in Seized Materials and Biological Specimens. United Nations Office on Drugs and Crime, **2009**. https://www.unodc.org/unodc/en/scientists/guidance-for-the-validation-of-analytical-methodology-and-calibration-of-equipment.html (Accessed 2023-01-10).

(56) Jenkins, R.; Duggan, J. X.; Aubry, A. F.; Zeng, J.; Lee, J. W.; Cojocaru, L.; Dufield, D.; Garofolo, F.; Kaur, S.; Schultz, G. A.; Xu, K.; Yang, Z.; Yu, J.; Zhang, Y. J.; Vazvaei, F. Recommendations for Validation of LC-MS/MS Bioanalytical Methods for Protein Biotherapeutics. *AAPS J.* **2015**, 17, 1-16. DOI: 10.1208/s12248-014-9685-5

(57) Phillips, T. Affinity Chromatography in Antibody and Antigen Purification. In *Handbook of Affinity Chromatography*, 2nd ed.; CRC Press, **2005**; pp 367-389. DOI:10.1201/9780824751982.

(58) Jones, R. G.; Landon, J. Enhanced Pepsin Digestion: A Novel Process for Purifying Antibody $F(ab')_2$ Fragments in High Yield from Serum. *J. Immunol. Methods* **2002**, 263, 57-74. DOI: 10.1016/s0022-1759(02)00031-5

(59) De Jonge, N.; Peckys, D. B.; Kremers, G. J.; Piston, D. W. Electron Microscopy of Whole Cells in Liquid With Nanometer Resolution. *Proc. Natl. Acad. Sci. U S A* **2009**, 106, 2159-2164. DOI: 10.1073/pnas.0809567106

(60) Bechelany, M.; Maeder, X.; Riesterer, J.; Hankache, J.; Lerose, D.; Christiansen, S.; Michler, J.; Philippe, L. Synthesis Mechanisms of Organized Gold Nanoparticles: Influence of Annealing Temperature and Atmosphere. *Crystal Growth & Design* **2010**, 10, 587-596. DOI: 10.1021/cg900981q

(61) Huang, Y. M.; Hu, W.; Rustandi, E.; Chang, K.; Yusuf-Makagiansar, H.; Ryll, T. Maximizing Productivity of CHO Cell-Based Fed-Batch Culture Using Chemically Defined Media Conditions and Typical Manufacturing Equipment. *Biotechnol. Prog.* **2010**, 26, 1400-1410. DOI: 10.1002/btpr.436

(62) New England BioLabs. Protein Data in Escherichia coli. https://www.neb.com/tools-and-resources/usage-guidelines/protein-data (Accessed 2023-01-10).

(63) DrugBank Online. Trastuzumab. https://go.drugbank.com/drugs/DB00072 (Accessed 2023-01-10).

(64) DrugBank Online. Bevacizumab. https://go.drugbank.com/drugs/DB00112 (Accessed 2023-01-10).

(65) Pierpont, T. M.; Limper, C. B.; Richards, K. L. Past, Present, and Future of Rituximab-The World's First Oncology Monoclonal Antibody Therapy. *Front. Oncol.* **2018**, 8, 163. DOI: 10.3389/fonc.2018.00163

(66) DrugBank Online. Rituximab. https://go.drugbank.com/drugs/DB00073 (Accessed 2023-01-10).

(67) Ferris, R. L. et al. Nivolumab for Recurrent Squamous-Cell Carcinoma of the Head and Neck. *N. Engl. J. Med.* **2016**, 375, 1856-1867. DOI: 10.1056/NEJMoa1602252

(68) Abcam. Anti-HER2 ELISA Kit (ab237645). https://www.abcam.com/her2-elisa-kit-ab237645.html (Accessed 2023-01-10).

(69) ThermoFisher Scientific. IgG (Total) Human ELISA Kit. https://www.thermofisher.com/elisa/product/IgG-Total-Human-ELISA-Kit/BMS2091 (Accessed 2023-01-10).

For Table of Contents Only